Local and trajectory-based indexes for task-related energetic performance optimization of robotic manipulators

Fabrizio Vidussi[1] Paolo Boscariol[2],* Lorenzo Scalera [1]
Alessandro Gasparetto[2]

[1]DTG, Università degli Studi di Padova, Italy
[2]DPIA, Università degli Studi di Udine, Italy

Abstract

In this paper a task-dependent energetic analysis of robotic manipulators is presented. The proposed approach includes a novel performance index, which relates the energy consumption of a robotic manipulator to its inertia ellipsoid. To validate the method, the dynamic and electro-mechanic models of a 3-DOF SCARA robot are implemented and the influence of the location of a predefined point-to-point task (such as a pick-and-place operation) within the robot workspace is considered. The task-dependent analysis provides energy consumption maps that are compared with the prediction of the theoretical formulation based on the proposed Trajectory Energy Index (TEI), which can be used to optimally locate the task to obtain minimal energy consumption without having to compute it through extensive dynamic simulations. Results show the effectiveness of the method and the good agreement between the TEI and the effective energy consumption within the whole workspace of the robot for several trajectories.

1 Introduction

Nowadays, industry is facing the challenge of implementing cost-effective and energy-efficient processes. These requirements are driven not only by economic considerations, but also by environmental politics, such as those set by the European Union [1]. The manufacturing industry is already responsible for a large percentage of the overall global energy consumption [2], and such a figure is expected to increase according to the foreseen growing of the worldwide demand of industrial robots [3]. In this scenario, engineers and researchers are investigating several solutions for energy efficiency, which allow robots to work with lower production costs without affecting productivity. An extensive review of the several methods that can contribute to energy saving in robotic and mechatronic devices is presented in [4].

Strategies to increase the energetic performance include the design of lightweight mechanical components and links [5], the adoption of regenerative drives [6], and the exploitation of the system natural dynamics [7, 8]. Adding springs and reaction wheels can sensibly reduce the power consumption of robots [9, 10] [11] associated with a simple task. However, this kind of modifications can be troublesome in industrial practice. Further approaches to decrease the energy or torque required by robots actuators include the re-scheduling of operations, the optimization of motion time, and the planning of optimal paths and trajectories [12]. For example, in [13] a trajectory planning approach for the energy saving in a redundant robotic cell is presented, whereas in [14] the effects of different motion profiles for a single degree-of-freedom mechanical system on its over-

*corresponding author: paolo.boscariol@unipd.it

This is a pre-print of the article: F. Vidussi, P. Boscariol, L. Scalera, A. Gasparetto
Local and trajectory-based indexes for task-related energetic performance optimization of robotic manipulators
Journal of Mechanisms and Robotics, 2021, 13.2: 021018 https://doi.org/10.1115/1.4049972

all energy consumption are taken into account using analytic methods. Other examples can be found in [15], where time and energy-optimal trajectories are analyzed for the pick-and-place motion of a 6-DOF robot, and in [16], where simple motion trajectories are employed for the energy saving in industrial machines.

The behavior of industrial manipulators can be estimated by adopting local and global performance measures and indexes. The study of these measures is motivated by the fact that local performance indexes can be used to define the relationship between robot and task definition. Furthermore, local performance indexes can provide guiding principles in the relative positioning of robot and task, as well as an analysis of the areas of the workspace in which the robot performance are maximized [17]. Early examples of performance indexes are based on the concept of generalized inertia ellipsoid [18], introduced by Asada in 1984 to study the mass properties and dynamic behavior of robotic arms, and on the manipulability index [19], proposed by Yoshikawa as a kinematic performance measure. Furthermore, in [20] the authors investigated dexterity measures of a manipulator based on its Jacobian matrix. Relevant examples of performance indexes can be found in [21], where measures for the quantification of dexterity of kinematically redundant manipulators are proposed, and in [22], where performance indexes are applied to a SCARA robot and graphically evaluated.

Dexterity and other Jacobian-based performance metrics are however affected by the dimensional inconsistency that arises whenever the robot has both rotational and translational degrees of freedom. One example is [23], in which a dimensionally homogeneous Jacobian matrix is used to design the optimal configuration of parallel manipulators for the best dexterity, thus proving a solution to the unit inconsistency of standard methods. The authors in [24] proposed numerical formulation of the velocity equation for any topology of spatial mechanism, again using a dimensionless Jacobian matrix, whereas in [25] dimensionless Jacobian matrices are formulated for the dexterity analysis of parallel manipulators regardless of the number and type of degrees of freedom of the mechanism. Furthermore, in [26] a performance index given by the inverse of the condition number is used to measure the motion performance of a 2-DOF spherical wrist. In [27] Jacobian, manipulability, condition number, and accuracy are analyzed and applied to parallel robots, exposing the limits of Jacobian-based performance indexes for this kind of robots.

Further performance indexes are examined for the optimal design of redundantly actuated parallel robots in [28], cable-driven robots in [29, 30], and for the optimal choice of large workspace robots in [31].

Several other studies are worth of mention for having analyzed some task-related rather than local (i.e. punctual) performance metric of a manipulator In [32] the authors derived a relationship between joint velocity and end-effector acceleration, and through case studies demonstrated that velocity has a complex, non-negligible effect on manipulability. In [33] the inertia matching ellipsoid is proposed as a new index of dynamic performance for serial-link manipulator, and its effectiveness is demonstrated experimentally through the application to a pick-and-place operation. In [34] the authors investigated the relation between mechanical power and manipulability as a key element of the manipulator analysis, establishing a performance index to compute the optimal task positioning. Another example of task-dependent analysis can be found in [35], where a performance index is introduced to optimize the location of a pick-and-place task for a 4-DOF industrial parallel robot. The work [36] is also worth of mention, since it provides an in-depth analysis of the relationship between energy consumption, shaking force magnitude, peak motor torque and location of the robotic task to be executed for the case of an Orthoglide robot. The work concludes that the optimal location is in proximity of the isotropic configuration, but a general rule is unavailable for complicated tasks or irregular workspaces.

As seen so far, robot performance indexes are usually related to dexterity, manipulability, force or speed exertion capability. To the best of the author's knowledge, no performance indexes focused on energy consumption can be found in the present literature. In this paper a task-dependent energetic analysis of industrial manipulators based on the concept

This is a pre-print of the article: F. Vidussi, P. Boscariol, L. Scalera, A. Gasparetto
Local and trajectory-based indexes for task-related energetic performance optimization of robotic manipulators
Journal of Mechanisms and Robotics, 2021, 13.2: 021018 https://doi.org/10.1115/1.4049972

of inertia ellipsoid is provided, extending the preliminary analysis published in [37]. The effect of path and trajectory planning design on the overall energy consumption of a robot are evaluated for a given operation, such as a common pick-and-place task defined by a point-to-point motion in the joint space or in the operational space of the robot. A 3-DOF SCARA robot is considered and its dynamic and electro-mechanic models are developed. The influence of the location of the task within the robot workspace and the choice of the motion law are evaluated, providing an energy consumption map for each considered trajectory. The energy consumption maps are then compared with the prediction of the theoretical formulation based on the inertia ellipsoid according to the novel performance index. The main contributions of this work are: (a) the definition of a novel performance index, named Trajectory Energy Index (TEI), which relates the energy consumption of the manipulator to the inertia ellipsoid, and (b) the evaluation of a method based on inertia ellipsoid to measure the energetic performance of industrial manipulators with respect to a specific point-to-point motion. Despite there is a link between the proposed index and other concepts, such as the manipulability ellipsoid, the definition of the TEI remains a novel contribution compared to existing concepts and techniques already published in the literature.

The rest of the paper is organized as follows: in Section 2 the theoretical formulation of the proposed approach based on inertia ellipsoid is described. In Section 3 the dynamic and electro-mechanic robot models are presented, which are the used in Section 4 to provide an evaluation of the agreement between the prediction of the proposed performance indexes and the estimated energy consumption. The conclusions are given in Section 5.

2 Inertia ellipsoid and energetic performance measure

In this section, the theoretical formulation of the proposed performance index, based on the concept of inertia ellipsoid, is presented. The first part of the section deals with the geometric features that relate the proposed index with the energy consumption. Then, the analytical expression of this index is derived.

2.1 Geometric derivation

The kinetic energy $\mathcal{K}$ of a robotic system composed of n rigid links and n motors can be represented as a function of the $n-$dimensional joint velocity vector $\dot{\mathbf{q}}$ and of the $(n \times n)$ inertia matrix $\mathbf{M}$, according to the following equation:

$$\mathcal{K}(\mathbf{q}, \dot{\mathbf{q}}) = \frac{1}{2}\dot{\mathbf{q}}^T \mathbf{M}(\mathbf{q})\dot{\mathbf{q}} \tag{1}$$

The relationship between the energy associated with the execution of a task and the parameters that identify the positioning of that task in the operational space, which is the focus of [37], can be analyzed otherwise by representing the kinetic energy as a function of the end-effector pose $\mathbf{p}$ and velocity $\dot{\mathbf{p}}$ in the operational space. In order to do this, it is convenient to exploit the concept of generalized inertia tensor presented in [18]: to do this, the expression of the kinetic energy in (1) can be rewritten in terms of the end-effector velocity, $\dot{\mathbf{p}}$ rather than on the joint velocity vector $\dot{\mathbf{q}}$, using the inverse differential equation $\dot{q} = \mathbf{J}^{-1}\dot{\mathbf{p}}$:

$$\mathcal{K} = \frac{1}{2}\,\dot{\mathbf{p}}^T \mathbf{J}^{-T}\mathbf{M}\mathbf{J}^{-1}\dot{\mathbf{p}} \tag{2}$$

where the (6×1) vector $\mathbf{p}$ represents the pose of the end-effector in the operational space and $\mathbf{J}$ is the $(6 \times n)$ geometric Jacobian matrix of the manipulator. Thus, a new inertia matrix can be define in the operative space as:

$$\mathbf{G} = \mathbf{J}^{-T}\mathbf{M}\mathbf{J}^{-1} \tag{3}$$

Since by definition the kinetic energy is a positive defined function, $\mathbf{G}$ is a positive definite matrix and it depends only on the instantaneous robotic configuration (i.e., the joint pose vector $\mathbf{q}$).

Now, the case of a generic 2-DOF robot that might comprise both revolute and prismatic joints is considered to provide a simple example, that has also the benefit of allowing a simple and straightforward visual representation of the results. The formulation

This is a pre-print of the article: F. Vidussi, P. Boscariol, L. Scalera, A. Gasparetto
Local and trajectory-based indexes for task-related energetic performance optimization of robotic manipulators
Journal of Mechanisms and Robotics, 2021, 13.2: 021018 https://doi.org/10.1115/1.4049972

is however general, and what follows applies, with the obvious modifications, to any robot. Referring again to a 2-DOF robot the kinetic energy can be represented as a quadratic surface in a 3-D Euclidean space and the isoenergetic curves correspond to bi-dimensional ellipsoids in the plane $\mathcal{K} = \overline{\mathcal{K}}$, according to:

$$\overline{\mathcal{K}} = \frac{1}{2}\,\dot{\mathbf{p}}^T \mathbf{G} \dot{\mathbf{p}} = \text{constant} \tag{4}$$

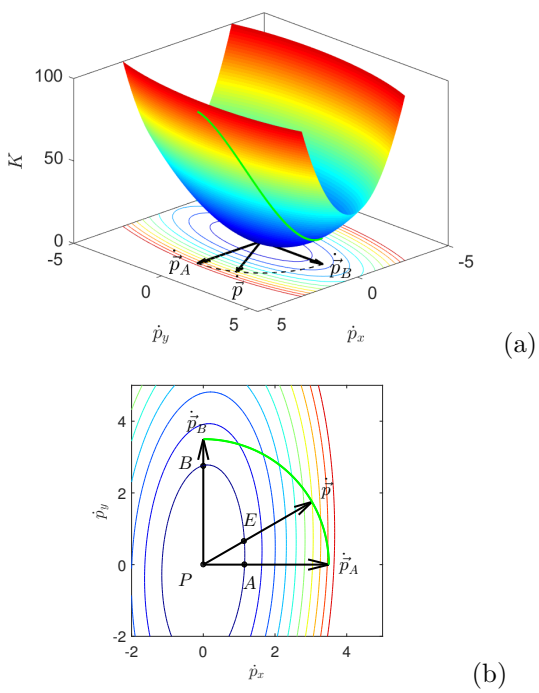

Figure 1: Kinetic energy surface (a) and inertia ellipsoid (b). The inverse of distance between the center P and a generic point E on the ellipsoid can be interpreted as a measure of the inertia of the robot when moving in the direction identified by the segment $\overline{PE}$.

For each energetic level $\overline{\mathcal{K}}$, the two principal axes of the ellipsoid can be obtained by solving the eigenvalue problem for matrix $\mathbf{G}$, since the length of the major axis a and of the minor axis b are related to the eigenvalues λ_1 and λ_2 of $\mathbf{G}$, as $a = 1/\sqrt{\lambda_1}$ and $b = 1/\sqrt{\lambda_2}$, and the directions of these axes are identified by the eigenvectors $\mathbf{v}_1$ and $\mathbf{v}_2$ of $\mathbf{G}$. These curves are also known as inertia ellipsoids. Figure 1(a) represents the energy as a generic quadratic surface, and the projection of the isoenergy curves on the velocity plane as ellipsoids. The center P of these ellipsoids corresponds to the instantaneous position of the robot end-effector. Let us consider two velocity vectors $\dot{\mathbf{p}}_A$ and $\dot{\mathbf{p}}_B$, parallel to the principal axes of the contour ellipses in Fig. 1(b). These vectors have the same norm but different directions, chosen so that the kinetic energy associated with $\dot{\mathbf{p}}_A$ is the largest one and the one associated with $\dot{\mathbf{p}}_B$ is the smallest one, as shown by the green curve on the surface. The corresponding kinetic energy values $\mathcal{K}_A$ and $\mathcal{K}_B$ can be expressed as:

$$\mathcal{K}_A = h_A(\mathbf{p}, \dot{\mathbf{p}})\,||\dot{\mathbf{p}}_A||^2 > \mathcal{K}_B = h_B(\mathbf{p}, \dot{\mathbf{p}})\,||\dot{\mathbf{p}}_B||^2 \tag{5}$$

where h_A and h_B are the scalar values of the generalized moment of inertia of the robot moving along $\dot{\mathbf{p}}_A$ and $\dot{\mathbf{p}}_B$, respectively. The generalized moment of inertia h depends on the robot configuration and on its velocity, and, therefore, on the direction of motion. Since $||\dot{\mathbf{p}}_B|| = ||\dot{\mathbf{p}}_A||$, it must be $h_A < h_B$. For the generic velocity vector $\dot{\mathbf{p}}$ with $||\dot{\mathbf{p}}|| = ||\dot{\mathbf{p}}_A||$, the generalized moment of inertia h can be found as $h\,(\mathbf{p}, \dot{\mathbf{p}}) = \mathcal{K}/||\dot{\mathbf{p}}_A||^2$, and $h_B \leq h \leq h_A$, being $\mathcal{K}_B \leq \mathcal{K} \leq \mathcal{K}_A$.

The energetic anisotropy described above can also be interpreted as suggested by the graphic representation reported in Fig. 1(b). In the figure, the intersections between the velocity vectors and the innermost ellipsoid define three points, A, B, E and three segments, $\overline{PA}$, $\overline{PB}$, $\overline{PE}$. When the motion is aligned with the major axis of the ellipsoid, i.e., $\overline{PB}$, the energy and the inertia take the minimum values, whereas when the motion is performed along the ellipsoid minor axis, i.e., $\overline{PA}$, the energy and the inertia take the largest values. Therefore, the generalized inertia moment is proportional to the inverse of the distance between the end-effector position P and the generic point E that identifies the direction of motion on the ellipsoid: $h \propto ||P - E||^{-1}$. Accordingly, a Local Energy Index (LEI) can be defined as:

$$LEI(\mathbf{q}, \dot{\mathbf{q}}) = \frac{1}{||P - E||} \tag{6}$$

The minimization of such index ensures that the

This is a pre-print of the article: F. Vidussi, P. Boscariol, L. Scalera, A. Gasparetto
Local and trajectory-based indexes for task-related energetic performance optimization of robotic manipulators
Journal of Mechanisms and Robotics, 2021, 13.2: 021018 https://doi.org/10.1115/1.4049972

direction of the end-effector motion occurs with the minimum generalized moment of inertia. The index allows to identify the most energy-efficient direction of the motion for each position of the end-effector in the plane. The LEI only depends on the joint configuration and on the direction of the motion, and it corresponds to the square of the eigenvalues of matrix $\mathbf{G}$, when the instantaneous velocity vector is aligned with the principal axes of the ellipsoid. The LEI is a local index, i.e., it is a function of the joint coordinates $\mathbf{q}$. However, the aim of this work is to define an index that measures the robot performance along a point-to-point trajectory $\dot{q}(t)$ with $t \in [t_0, t_f]$. To do so, a different performance index is defined as the Trajectory Energy Index (TEI):

$$TEI = \frac{1}{t_f - t_0} \int_{t_0}^{t_f} LEI(t)dt =$$

$$= \frac{1}{t_f - t_0} \int_{t_0}^{t_f} \frac{1}{||P(t) - E(t)||} dt \tag{7}$$

Since this index is proportional to the energy, being the mean value of the LEI, it can be used to relate a desired trajectory with the corresponding energy required by the manipulator. In this way, a minimization of the TEI can be used in the design of energy-efficient point-to-point motions. It must be pointed out that this relationship is valid without any modification to the proposed formulation in all cases in which the effects of gravity on energy consumption is independent of the robot motion, as in the case of null or homogeneous effects of gravity load.

2.2 Analytic expression for planar motion

In this section, the analytical expression of the first proposed index is derived and analyzed, considering a generic 2-DOF planar manipulator. Figure 2 shows that the inertia ellipsoid is centered on point P, which belongs to the trajectory s. The reference frame $\{X^P, Y^P\}$ has the same orientation of the robot base reference frame. The line γ is tangent

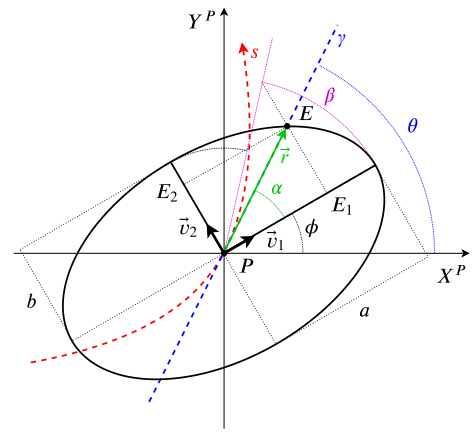

Figure 2: Inertia ellipsoid corresponding to the point P of the trajectory s for a generic planar manipulator with 2-DOF. The vector $\mathbf{g}$ has the same direction θ of the movement in the point P and module equal to the inverse of the energetic performance index proposed.

to the trajectory s at point P, and defines the instantaneous direction θ of the motion. As previously explained, the directions of the principal axes of the ellipsoid are identified by the eigenvectors $\mathbf{v}_1$ and $\mathbf{v}_2$ of $\mathbf{G}$, and the corresponding dimensions a, b are related to the eigenvalues λ_1 and λ_2 of $\mathbf{G}$. The angle ϕ represents the orientation of the ellipsoid major axis and can be evaluated using the first eigenvector $\mathbf{v}_1$ as $\phi = \arctan(v_{1,y}/v_{1,x})$.

The intersection point E between the ellipsoid and the tangent line γ defines the vector $\mathbf{r}$, which has the same direction of the motion θ and module equal to the length of segment $\overline{PE}$. This length can be derived from the projections of the point E on the principal axes of the ellipsoid, i.e., E_1 and E_2, as $||\mathbf{g}|| = \sqrt{E_1^2 + E_2^2}$. Then, according to Eq. (6), the LEI is equal to the inverse of the module of $\mathbf{r}$ and its two components are related to the axis length a, b, and to the angle β as follows:

$$\begin{cases} E_1 = a\cos\beta \\ E_2 = b\sin\beta \end{cases} \tag{8}$$

In order to evaluate β, the direction α of the vector

This is a pre-print of the article: F. Vidussi, P. Boscariol, L. Scalera, A. Gasparetto
Local and trajectory-based indexes for task-related energetic performance optimization of robotic manipulators
Journal of Mechanisms and Robotics, 2021, 13.2: 021018 https://doi.org/10.1115/1.4049972

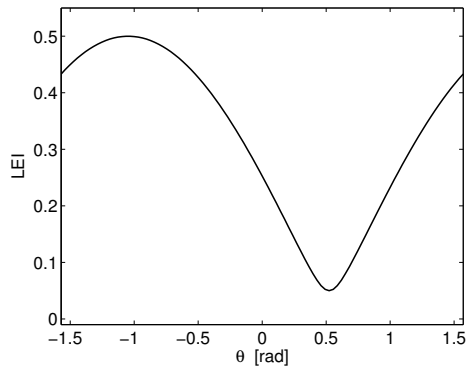

Figure 3: The Local Energy Index as a function of the direction θ according to Eq. (11), when $a = 20$, $b = 2$ and $\phi = \pi/6$. The minimum is obtained when $\theta = \phi$, i.e., when the movement is aligned with the ellipsoid major axis.

$\mathbf{r}$ in the ellipsoid reference frame can be exploited:

$$\begin{cases} \theta = \phi + \alpha \\ \alpha = \arctan\left(\dfrac{E_2}{E_1}\right) = \arctan\left(\dfrac{b}{a}\tan\beta\right) \end{cases} \tag{9}$$

leading to:

$$\beta = \arctan\left(\frac{a}{b}\tan(\theta - \phi)\right) \tag{10}$$

Finally, the LEI can be written as:

$$\mathrm{LEI} = \left[a^2\cos^2\left(\arctan\left(\frac{a}{b}\tan(\theta-\phi)\right)\right) + b^2\sin^2\left(\arctan\left(\frac{a}{b}\tan(\theta-\phi)\right)\right)\right]^{-1/2} \tag{11}$$

One can notice that, as long as the position of the end-effector in the workspace is chosen, the parameters a, b and ϕ are unequivocally identified, since the matrix $\mathbf{G}$ depends on the robot configuration only. Then, the only degree of freedom is the direction of the movement θ. Furthermore, the minimum of the LEI is found for $\theta = \phi$, i.e., the movement is aligned with the ellipsoid major axis, and $\min(\mathrm{LEI}) = 1/a$. Figure 3 shows the LEI as a function of θ for $a = 20$, $b = 2$ and $\phi = \pi/6$. This applies for the given values of $\mathbf{q}$ and $\dot{\mathbf{q}}$, but it can be seen that the minimum value of the TEI, which identifies the approximation of the energetic optimal trajectory, can be obtained by minimizing the mean value of the LEI.

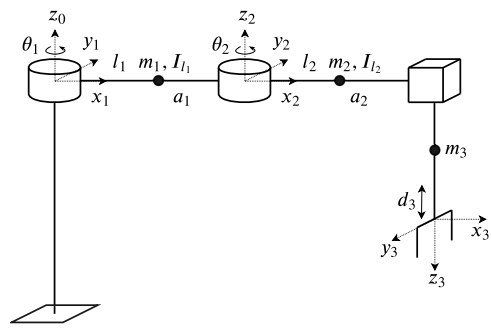

Figure 4: SCARA robot: kinematic definitions and mass distribution.

3 Robot model

In this section the model of the robot used as the test-bench is presented: first its dynamic model of the robot and then the electro-mechanical model of the actuators are explained. Finally, the power losses model is define by taking into account all the relevant losses.

3.1 Dynamic model

A 3-DOF SCARA robot designed according to the common RRP architecture is shown in Fig. 4. Its geometric Jacobian matrix $\mathbf{J}$ can be computed as:

$$\mathbf{J} = \begin{bmatrix} -a_1 s_1 - a_2 s_{12} & -a_2 s_{12} & 0 \\ a_1 c_1 + a_2 c_{12} & a_2 c_{12} & 0 \\ 0 & 0 & -1 \\ 0 & 0 & 0 \\ 0 & 0 & 0 \\ 1 & 1 & 0 \end{bmatrix} \tag{12}$$

where $s_1 = \sin\theta_1$, $c_1 = \cos\theta_1$, $s_{12} = \sin(\theta_1 + \theta_2)$, $c_{12} = \cos(\theta_1 + \theta_2)$, a_i is the length of the i-th link, whereas θ_1, θ_2 are the first two joints variables.

This is a pre-print of the article: F. Vidussi, P. Boscariol, L. Scalera, A. Gasparetto
Local and trajectory-based indexes for task-related energetic performance optimization of robotic manipulators
Journal of Mechanisms and Robotics, 2021, 13.2: 021018 https://doi.org/10.1115/1.4049972

In order to provide a realistic evaluation of the energy consumption and the corresponding energetic performance index, the inverse dynamic problem must be solved. For this purpose, once the geometric and mass properties of arms and motors are defined, given the vectors of position $\mathbf{q}$, velocity $\dot{\mathbf{q}}$ and acceleration $\ddot{\mathbf{q}}$ of the joints, it is possible to exploit the Lagrangian formalism to compute the joint torque vector τ. First of all, the kinetic energy $\mathcal{K}$ and the potential energy $\mathcal{U}$ are use to calculate the Lagrangian function $\mathcal{L} = \mathcal{K} - \mathcal{U}$ of the system. Then, the joint torque vector τ is obtained through the Lagrange equation:

$$\frac{d}{dt}\frac{\partial \mathcal{L}}{\partial \dot{\mathbf{q}}} - \frac{\partial \mathcal{L}}{\partial \mathbf{q}} = \tau\left(\mathbf{q}, \dot{\mathbf{q}}, \ddot{\mathbf{q}}, t\right) \tag{13}$$

The kinetic energy $\mathcal{K}$ is computed as in Eq. (1), and the inertia matrix $\mathbf{M}$ can be represented as follows:

$$\begin{aligned}\mathbf{M}(\mathbf{q}) = \sum_{i=1}^{n} \Big(& m_{l_i} \mathbf{J}_P^{(l_i)T} \mathbf{J}_P^{(l_i)} + \mathbf{J}_O^{(l_i)T} \mathbf{I}_{l_i} \mathbf{J}_O^{(l_i)} \\ & + m_{m_i} \mathbf{J}_P^{(m_i)T} \mathbf{J}_P^{(m_i)} + \mathbf{J}_O^{(m_i)T} \mathbf{I}_{m_i} \mathbf{J}_O^{(m_i)} \Big)\end{aligned} \tag{14}$$

m_{l_i} is the mass of the link i, $\mathbf{I}_{l_i}$ is the inertia tensor relative to the center of mass of link i, m_{m_i} is the mass of the motor i, $\mathbf{I}_{m_i}$ is the inertia tensor of the rotor i, whereas $\mathbf{J}_P$ and $\mathbf{J}_O$ are the position and orientation geometric Jacobian matrices respectively, for each link l_i and motor m_i. By using a lumped mass model parameters, the inertia moment of link i referred to the z axis of the i-th frame can be calculated as $I_{l_i} = 1/2 m_{l_i} l_i^2$. The values of motors inertia moment with respect to the rotor axis are reported in Tab. 1. The potential Energy $\mathcal{U}$ can be evaluated as:

$$\mathcal{U} = g \sum_{i=1}^{n} (m_{l_i} p_{z,l_i} + m_{m_i} p_{z,m_i}) \tag{15}$$

where g is the gravity constant, and p_{z,l_i} and p_{z,m_i} are the height of link i and motor i referred to the base reference frame, respectively. Accordingly, for the 3-DOF SCARA under study, the only meaningful contribution to the potential energy is due to the third link, since the motion of the last joint is orthogonal to the other motions.

By applying Eq. (13) to the expression of kinetic and potential energy just explained, the joint torques can be evaluated. In order to consider also the non-conservative forces, viscous friction force $\mathbf{F}_v \dot{\mathbf{q}}$ and Coulomb friction force $\mathbf{f}_c = f_c \operatorname{sgn}(\dot{\mathbf{q}})$ are added to the conservative torque vector τ. Then, the dynamics of the robot can be expressed as:

$$\tau = \mathbf{M}(\mathbf{q})\ddot{\mathbf{q}} + \mathbf{C}(\mathbf{q}, \dot{\mathbf{q}})\dot{\mathbf{q}} + \mathbf{F}_v \dot{\mathbf{q}} + f_c \operatorname{sgn}(\dot{\mathbf{q}}) + \mathbf{g}(\mathbf{q}) \tag{16}$$

where $\mathbf{M}$ is the inertia matrix of Eq. (14) , $\mathbf{C}$ is the matrix of Coriolis and centripetal non-linear forces:

$$\mathbf{C} = \begin{bmatrix} \epsilon\, \dot{\theta}_2 & \epsilon \left(\dot{\theta}_1 + \dot{\theta}_2\right) & 0 \\ -\epsilon\, \dot{\theta}_1 & 0 & 0 \\ 0 & 0 & 0 \end{bmatrix} \tag{17}$$

where $\epsilon = -a_1 s_2 (l_2 m_{l_2} + a_2 m_{l_3} + h_2 m_{m_3})$, and $\mathbf{g} = [0 \quad 0 \quad -g m_{l_3}]^T$ is the gravitational force vector.

3.2 Electro-mechanic model

In this section the electro-mechanical model of the robot actuators is presented. This model aims at calculating the voltages and the currents that must be provided to the motors to obtain the desired velocity $\dot{\mathbf{q}}_m$ and torque τ_m. Currents and voltages are used to computed the energy required to perform a motion task.

First of all, the joint velocity and the joint torque profiles given by the trajectory planning algorithm and the by inverse dynamics in Eq. (16), are reduced to the motor axis taking into account the gearboxes. Assuming that harmonic drives are used for the two revolute joints, and a screw ball is use to covert the rotational motion of the third motor into a linear motion, velocity and torque values at the motor side can be expressed as:

$$\begin{cases} \dot{\mathbf{q}}_m = \mathbf{K}_r \dot{\mathbf{q}} \\ \tau_m = \eta_r \mathbf{K}_r^{-1} \tau \end{cases} \tag{18}$$

where $\mathbf{K}_r$ is the diagonal matrix of the gear reduction ratios k_{r_i}, and η_r is the diagonal matrix of the gear efficiencies η_{r_i}.

It is assumed that the robot is actuated by three surface permanent magnet synchronous motors. The

This is a pre-print of the article: F. Vidussi, P. Boscariol, L. Scalera, A. Gasparetto
Local and trajectory-based indexes for task-related energetic performance optimization of robotic manipulators
Journal of Mechanisms and Robotics, 2021, 13.2: 021018 https://doi.org/10.1115/1.4049972

electric model of each motor consists of three phase voltage equations that, under the hypothesis of linear and isotropic system, can be expressed as follows:

$$\begin{cases} u_a = & Ri_a + L\dfrac{di_a}{dt} + \dfrac{d\lambda_{a,mg}}{dt} \\ u_b = & Ri_b + L\dfrac{di_b}{dt} + \dfrac{d\lambda_{b,mg}}{dt} \\ u_c = & Ri_c + L\dfrac{di_c}{dt} + \dfrac{d\lambda_{c,mg}}{dt} \end{cases} \tag{19}$$

where u_x and i_x are the voltage and the current on the phase x, R and L are the resistance and the inductance of each stator winding, and $\lambda_{x,mg}$ is the flux due to the permanent magnet and linked by the x winding; deriving this flux in time gives the back EMF on the relative winding. By using the space vector representation and by applying Clarke and Park transformations [38], it is possible to rewrite the three-phase model of Eq. (19) as the following dq bi-phase model:

$$\begin{cases} u_d = & Ri_d + L\dfrac{di_d}{dt} - p_p\dot{q}_m i_q \\ u_q = & Ri_q + L\dfrac{di_q}{dt} + p_p\dot{q}_m i_d + p_p\dot{q}_m\Lambda_{mg} \end{cases} \tag{20}$$

where Λ_{mg} is the residual induction of the magnet and p_p is the number of pole pairs. Now it is possible to apply an energy balance procedure in order to find the relation between motor torque and current:

$$\tau_m = \frac{3}{2}p_p\Lambda_{mg}i_q = k_t i_q \tag{21}$$

which shows that the torque is proportional to the current i_q by the torque constant $k_t = \frac{3}{2}p_p\Lambda_{mg}$. Also on the basis of this last consideration, Eq. (20) can be further simplified. As a matter of fact, according to the space vector representation, the current i_{drive} that must be provided by the inverter can be written as: $|i_{drive}| = \sqrt{i_d^2 + i_q^2}$. This means that in order to match the maximum torque per ampere condition, the i_d current must be zero. In addition, since the electrical dynamics is often significantly faster with respect to the mechanical dynamics, it is conceivable to neglect current transients, i.e., the $L\,di/dt$ terms. Therefore, assuming that all these conditions are met and accounting for all actuators, the electro-mechanic model can be written as:

$$\begin{cases} \mathbf{u} = \mathbf{R}\mathbf{i} + \mathbf{K}_e\dot{\mathbf{q}}_m \\ \tau_m = \mathbf{K}_t\mathbf{i} \end{cases} \tag{22}$$

where $\mathbf{u}$ and $\mathbf{i}$ are the vector of q-axes voltage and current, $\mathbf{R}$ is the diagonal matrix of the winding resistances, $\mathbf{K}_e$ is the diagonal matrix of the back EMF constants $k_{e_i} = p_{p_i}\Lambda_{mg_i}$ and $\mathbf{K}_t$ is the diagonal matrix of torque constants.

3.3 Power losses model

The sources of the main power losses in industrial robots are now discussed. According to [39, 40], the main type of losses can be categorized as follows.
(1) Mechanical losses include viscous friction losses and Coulomb friction losses that are already included in the dynamic model of the robot.
(2) Motor losses encompass stator and rotor, iron and stray load losses. Stator and rotor losses, also known as i^2 losses, describe the joule energy dissipated by the motor winding resistance R, and are included in the electrical model of the actuators. Iron losses, due to magnetization and demagnetization of the windings, are heavily influenced by magnetic induction and its frequency of variation, and are typically very difficult to compute exactly. A common simplified model is based on the consideration that these losses vary with the motor speed and, therefore, can be interpreted as viscous losses, which can be included in the dynamic model by properly increasing the viscous friction coefficient. Stray load losses are related to flux leakage that occurs through the windings when the motor is operating under its specific load. These losses depend on the square value of the current and can be included in the i^2 losses by fictitiously increasing the winding resistance R.
(3) Motor drive losses are mainly composed of inverter, rectifier and DC-bus losses. Inverter losses, are resistive losses due to the inverter transistors switching frequency mainly, and therefore can be included in the i^2 losses category, as for the stray load losses. Rectifier losses and DC-bus losses are hard to model without a proper knowledge of their detailed

This is a pre-print of the article: F. Vidussi, P. Boscariol, L. Scalera, A. Gasparetto
Local and trajectory-based indexes for task-related energetic performance optimization of robotic manipulators
Journal of Mechanisms and Robotics, 2021, 13.2: 021018 https://doi.org/10.1115/1.4049972

electric schematics. Therefore, one possible choice is to collect all the motor drive losses within the efficiency η_d. The latter might be either represented as a constant value, or as a function of the driver duty cycle [41].

3.4 Energy consumption estimation

Once the voltage and current profiles of Eq. (22) are determined, given the parameters in Tab. 1, the total energy consumption E_{tot} can be computed as the time integral of the three-phase electric power drawn by the robot $\mathbf{P}_{d,tot}(t)$:

$$E_{tot} = \int_{t_i}^{t_f} \mathbf{P}_{d,tot}(t)\,dt = \int_{t_i}^{t_f} \frac{3}{2\eta_d}\mathbf{u}(t)^T\mathbf{i}(t)\,dt = \frac{3}{2\eta_d}\left(\int_{t_i}^{t_f} \mathbf{R}^T\mathbf{i}(t)\mathbf{R}\,dt + \int_{t_i}^{t_f} \dot{\mathbf{q}}_m^T(t)\mathbf{K}_e\mathbf{K}_t^{-1}\tau_m(t)\,dt\right) \tag{23}$$

The first term of the integral represents the Joule energy and the second accounts for the total electromechanic energy.

4 Results

The energetic model explained in the previous section is used to estimate the energy consumption of the robot in relation to the choice of the point-to-point motion law and to the positioning of the task within the robot workspace. For each motion profile, by varying the task parameters defined in the Cartesian space (as described below), the corresponding energy absorption is computed and the results are collected into energy maps. Following the same procedure, the energetic performance index is computed to create TEI maps that are compared with the energy values in order to evaluate the effectiveness of the proposed index.

4.1 Task-dependent energetic analysis

The task considered for the task-dependent analysis is the translation of the robot end-effector from a starting point P_i to a final point P_f, as performed in a pick-and-place operation. The path that connects the two points depends on the adopted motion law. Figure 5 shows the parameterization that is chosen to represent such a task on the $\{X, Y\}$ plane, where the origin of the reference system corresponds to the position of robot base. Given a fixed execution time and the total displacement Δ, three parameters are left free: the polar coordinates (d, ϕ) of the mid-point of the segment $\overline{P_iP_f}$ that represents the task, and its orientation θ with respect to the X axis. Though, due to the symmetry of the SCARA configuration around the Z axis, variations of ϕ do not affect energy absorption, as long as the task is performed away from the limits of the first joint. This allows to set $\phi = 0$. Hence, the task is unequivocally identified by the two parameters θ and d. According to the limits of the workspace, the orientation θ ranges from 0 rad to π rad, the distance d varies from 0.1 m to 0.7 m, whereas the displacement Δ is set to 0.28 m. The execution time is set to 0.8 s for all the tests.

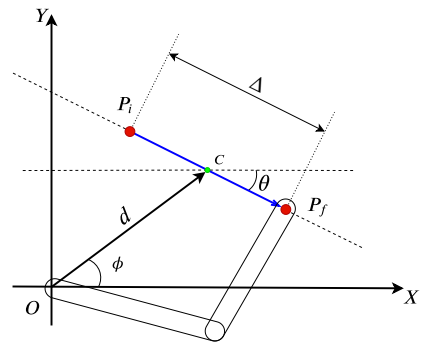

Figure 5: Path parameterization.

As far as the choice of the motion law is concerned, four well-known point-to-point trajectories are taken into account [42], i.e., the third and the fifth-order polynomial profile in the joint space, and the third and the fifth-order polynomial profile defined in the operational space, all designed for rest-to-rest motion. In the second case, the motion of the end-effector is forced to follow a straight line, since all the via points are imposed on the $\{X, Y\}$ plane. On the other hand, planning in the joint space allows the robot end-effector to perform arcs instead

This is a pre-print of the article: F. Vidussi, P. Boscariol, L. Scalera, A. Gasparetto
Local and trajectory-based indexes for task-related energetic performance optimization of robotic manipulators
Journal of Mechanisms and Robotics, 2021, 13.2: 021018 https://doi.org/10.1115/1.4049972

Table 1: Dynamic properties of the SCARA robot.

Parameter	**Joint 1**	**Joint 2**	**Joint 3**
a_i	0.35 m	0.35 m	-
m_{l_i}	9 kg	8 kg	1 kg
k_{r_i}	1/80	1/50	1/50
η_{r_i}	0.7	0.7	0.8
m_{m_i}	7.1 kg	6.3 kg	2.5 kg
I_{m_i}	$5 \cdot 10^{-4}$ kgm^2	$4 \cdot 10^{-4}$ kgm^2	$1 \cdot 10^{-4}$ kgm^2
f_v	$8 \cdot 10^{-4}$ Nms/rad	$7 \cdot 10^{-4}$ Nms/rad	$5 \cdot 10^{-4}$ Nms/rad
f_s	$2 \cdot 10^{-4}$ Nm	$2 \cdot 10^{-4}$ Nm	$2 \cdot 10^{-4}$ Nm
R_i	0.39 Ω	0.39 Ω	1.67 Ω
k_{e_i}	0.16 Vs/rad	0.16 Vs/rad	0.12 Vs/rad
k_{t_i}	0.28 Nm/A	0.28 Nm/A	0.21 Nm/A
η_d	0.9	0.9	0.9

of straight lines. This choice reflects the two options offered by virtually all robot manufacturers. The energy maps obtained according to the procedure previously described are shown in Fig. 6. Each map corresponds to one motion profile and the energy, expressed in Joule, is represented as a function of parameters (θ, d). The black lines indicate the isoenergetic curves in the (θ, d) plane. Figures 6(a),(b) show the results of motion tasks defined in the joint space, whereas Figs. 6(c),(d) refer to operative space planning. The location of the minimum for each maps is highlighted by a pink circle: their location in Fig. 6 suggest that, for the robot under investigation, high values of distance d and values of θ close to 2 rad are to be preferred whenever the reduction of the energy required to perform a rest-to-rest motion task is sought.

The comparison between Figs. 6(a),(b) and Figs. 6(c),(d) highlights that the size of the unfeasible area in the joint space map is smaller than in the case of operational space maps. This is due to the fact that, given two points in the robot workspace, a straight line that connects these two points and goes across the internal workspace boundaries is not feasible. On the other hand, an arc that connects the two points without violating the internal boundaries always exists. Additionally, despite the larger length of the end-effector path, the joint space energy maps (Figs. 6(a),(b)) present slightly lower energy levels than the corresponding operational space maps (Figs. 6(c),(d)), and as expected [13, 43] primitives defined by lower degree polynomials are more energetically efficient. Within each map, i.e., for any choice of the motion profile, the energy distribution varies quite heavily. Looking at Fig. 6(a) highlights that by changing the location of the task the energy required to provide a single point-to-point motion can vary from 38 J to over 50 J. Similar trends applies to the other maps. Hence, as in [37], it can be inferred that the location of the task within the robot workspace has a heavier impact on the energy consumption then the choice of the motion law itself.

The relation between task-positioning and energy is further highlighted in Fig. 7, which refers to the data already presented in Fig. 6(c). In this figure each arrow represents a motion task that connects its initial and final point within the robot workspace. The red arrows represent the optimal orientation θ of the path for 15 evenly spaced values of distance d from the base (for values from 0.33 m to 0.7 m). The blue arrow represents the overall optimal solution that corresponds to $\theta = 1.885$ rad, $d = 0.57$ m. This graphic representation suggests that, from the energetic point of view, the radial motion is the most efficient when operating close to the robot base, whereas a tangential motion is to be preferred when operating towards the external boundaries of the workspace. Similar considerations apply to the other three cases

This is a pre-print of the article: F. Vidussi, P. Boscariol, L. Scalera, A. Gasparetto
Local and trajectory-based indexes for task-related energetic performance optimization of robotic manipulators
Journal of Mechanisms and Robotics, 2021, 13.2: 021018 https://doi.org/10.1115/1.4049972

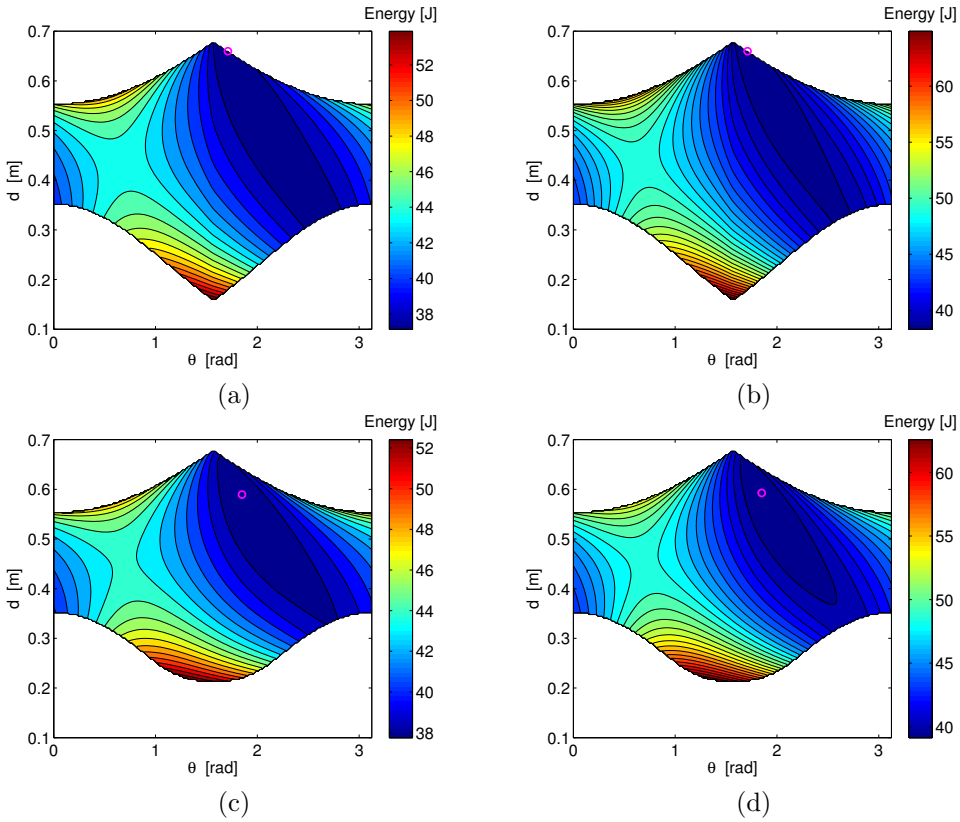

Figure 6: Energy consumption maps: poly3 (a) and poly5 (b) joint space planning, poly3 (c) and poly5 (d) operative space planning.

under investigation.

4.2 Energetic performance index evaluation

Finally, the evaluation of the Trajectory Energy Index is performed by computing the maps for the same tasks already analyzed and by comparing the results with the corresponding energy maps. Figure 8 shows the TEI function maps for the four previously analyzed motion laws. Red color is associated with higher values of TEI, blue color indicates lower values of TEI. The small pink circle represents the absolute minimum value of the TEI within each map. The first evidence, according to the direct comparison between Fig. 6 and Fig. 8, is the almost perfect overlap between the pink circles, which is evident when comparing each energy map with the corresponding TEI map. This feature suggests that the TEI can foreseen quite precisely the task associated with minimum energy expenditure.

Each energy map and the corresponding TEI map also show similar gradients, as can be seen, for example, by comparing Fig. 6(a) with Fig. 8(a). This implies that the TEI can be used to foreseen very well the energy variation in the (θ, d) plane, but it cannot be used alone to make a quantitative estimation of this energy. As consequence, the proposed index represents a good objective function to be used in any task optimization process, where the energy consumption has to be minimized. Opting for the choice of the TEI as the cost function to be mini-

This is a pre-print of the article: F. Vidussi, P. Boscariol, L. Scalera, A. Gasparetto
Local and trajectory-based indexes for task-related energetic performance optimization of robotic manipulators
Journal of Mechanisms and Robotics, 2021, 13.2: 021018 https://doi.org/10.1115/1.4049972

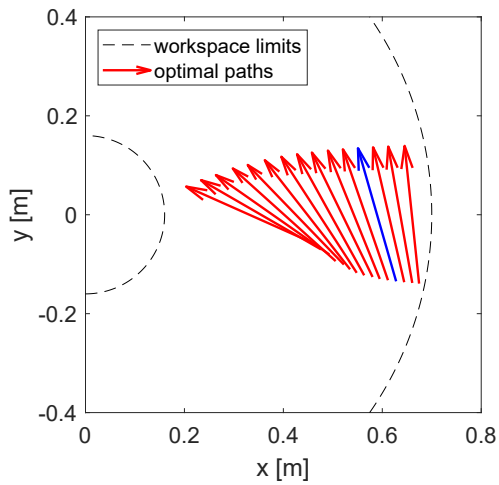

Figure 7: Optimal path orientation θ by varying the distance d from the base (for values from 0.33 m to 0.7 m) for the 3rd order polynomial profile in the operational space: the overall best solution is shown in blue color.

mized when planning an energy optimal motion task allows to avoid the computational burden imposed by the explicit solution of the inverse dynamics model and of the related computation of the current and voltages profiles. Therefore Eq. (14)-(18), (22) and (23) are not needed, and Eq. (3) and (7) can suffice. This statement is also supported by the data collected in Tab. 2, which reports the results of the energy minimization and of the TEI minimization. As far as the two tasks defined in the joint space are concerned, the two minima overlap perfectly. i.e., the minimization of the proposed energetic index brings the very same results obtained by minimizing the energy required to run the robot. When referring to motion tasks defined in the operative space, the two optima are located in slightly different locations of the (θ, d) plane, but the corresponding energy consumption vary at most by 0.38%. Such a small percentage represents a discrepancy that, however, is expected to be outscored by the uncertainties of the energy estimation model used here.

The relationship between the orientation of inertia ellipsoid with respect to the direction of motion and the corresponding energy consumption is clearly visible in Fig. 9. The sampled values of the end-effector path that correspond to the maximum (on the left) and to the minimum (on the right) energy consumption are represented by the red crosses, whereas the red circle indicates the robot base. The inertia ellipsoid are shown in blue, whereas the green arrows are the samples of $\mathbf{r}$ vector, described in Fig. 2. Dashed lines indicate the workspace limits. This figure corroborates the hypothesis that the more the trajectory is aligned to the ellipsoids major axis (i.e., the smallest the LEI values), the less energy is required to perform such a movement, and vice-versa. This also confirms the interpretation of the arrows graph (Fig. 7), according to which the radial and tangential motions are more energy-effective when performed close to and away from the robot base, respectively.

5 Conclusions

In this paper two novel performance indexes based on the concept of inertia ellipsoid are proposed as efficient tools for the analysis of the energy consumption of robotic manipulators executing simple motion tasks. The first performance index, i.e., the Local Energy Index, relates the direction of motion of the end-effector of the robot to its kinetic energy, whereas the other index, referred to as Trajectory Energy Index, extends this metric to a whole point-to-point trajectory. The TEI is used to evaluate the effects of the collocation of a simple motion task on the energy consumption of the robot, referring to a benchmark SCARA robot. The energy consumption of the robot is evaluated thorough a detailed dynamic and electro-mechanic model. Results show the effective agreement between the energy consumption maps and the TEI maps, computed for different point-to-point primitive trajectories, highlighting that the Trajectory Energy Index can be used with very little approximation to define the optimal minimum-energy task. Therefore, the proposed performance index significantly reduces the computational burden required to solve and integrate the robot dynamics.

The TEI can be used for practical task-dependent analysis of the energy consumption of a manipula-

This is a pre-print of the article: F. Vidussi, P. Boscariol, L. Scalera, A. Gasparetto
Local and trajectory-based indexes for task-related energetic performance optimization of robotic manipulators
Journal of Mechanisms and Robotics, 2021, 13.2: 021018 https://doi.org/10.1115/1.4049972

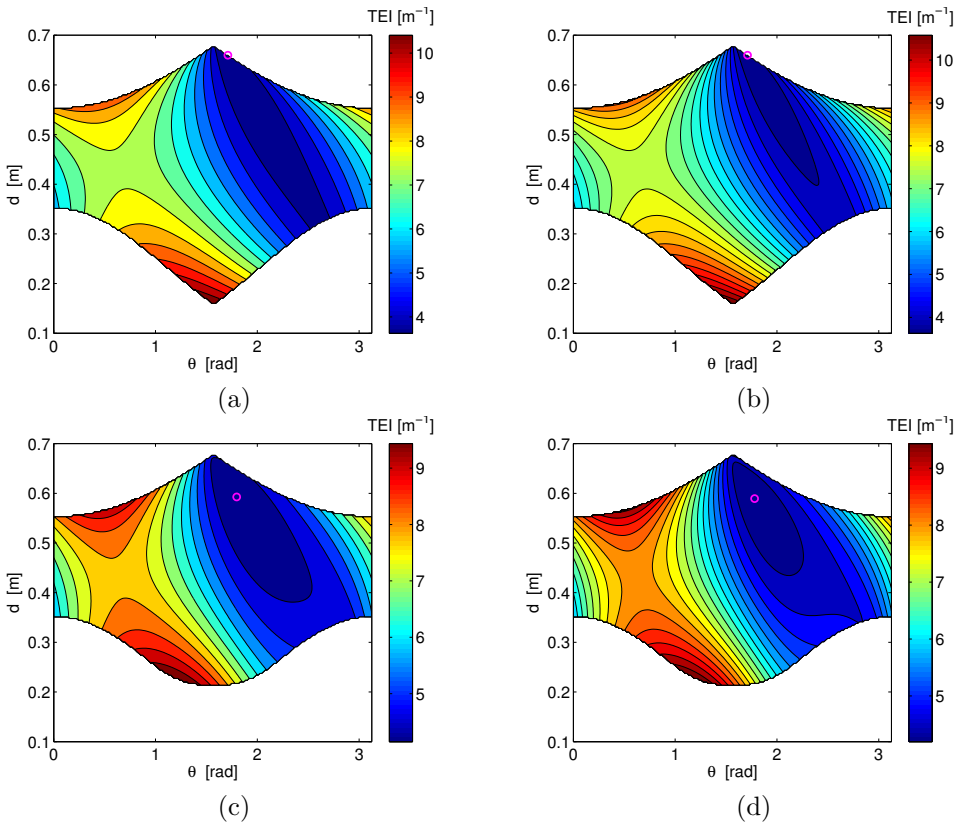

Figure 8: Trajectory Energy Index maps: poly3 (a) and poly5 (b) joint space planning, poly3 (c) and poly5 (d) operative space planning.

tor, for example when the layout of the plant or the robotic cell is designed. The method can give also practical indications about the most efficient location of a task: for a SCARA robot the radial motion is the most efficient when operating close to the robot base, whereas a tangential motion is to be preferred when operating towards the external boundaries of the workspace. The proposed performance index can also be used at the robot design stage, for example to maximize the performance in certain area of the workspace or by making it more uniform across the whole workspace.

The main limitation of the proposed index is that the formulation cannot take into account configuration-dependent contributions of gravitational force. Therefore, the applicability of the method is more meaningful when planar motions, during which gravity is constant, are considered. Furthermore, the trajectory optimization presented in the paper is only valid for point-to-point motions. Future developments of the work will include the extension of the proposed method to the case of non-constant gravity (i.e., in the spatial case), and to the case of generic multi-point and continuous trajectories.

References

[1] European Comission, 2012. Proposal for a directive of the European Parliament and of the

This is a pre-print of the article: F. Vidussi, P. Boscariol, L. Scalera, A. Gasparetto
Local and trajectory-based indexes for task-related energetic performance optimization of robotic manipulators
Journal of Mechanisms and Robotics, 2021, 13.2: 021018 https://doi.org/10.1115/1.4049972

Table 2: Minimum-energy and minimum-TEI solutions.

Task	**Min Energy** $[J]$	$\theta\,[rad]$	**d** $[m]$	**Min TEI**	$\theta\,[rad]$	**d** $[m]$	**Energy @ Min TEI** $[J]$
Poly3, joint space	37.14	1.71	.66	3.63	1.71	.66	37.14
Poly5, joint space	38.31	1.71	.66	3.66	1.71	.66	38.31
Poly3, operative space	37.74	1.85	.59	4.15	1.80	.59	37.82 (+0.21%)
Poly5, operative space	39.15	1.85	.59	4.19	1.78	.60	39.23 (+0.38%)

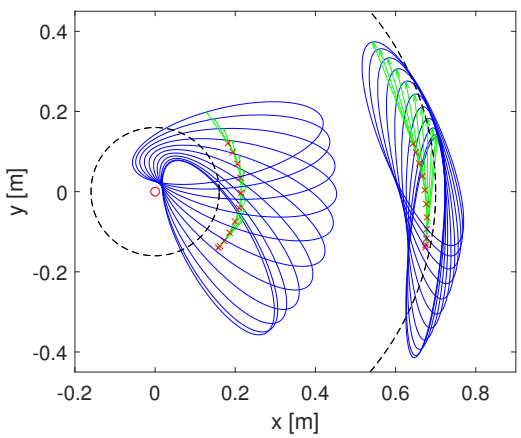

Figure 9: Inertia ellipsoids (in blue) in the robot workspace. The two tasks follow on average the minor and the major axes of the inertia ellipsoids respectively, according to the TEI definition.

council amending directive 2012/27/EU on energy efficiency. `https://eur-lex.europa.eu/homepage.html`.

[2] Kucukvar, M., Cansev, B., Egilmez, G., Onat, N. C., and Samadi, H., 2016. "Energy-climate-manufacturing nexus: New insights from the regional and global supply chains of manufacturing industries". *Applied energy,* **184**, pp. 889–904.

[3] International Federation of Robotics, 2019. Executive Summary World Robotics 2019 Industrial Robots. `https://ifr.org/free-downloads/`.

[4] Carabin, G., Wehrle, E., and Vidoni, R., 2017. "A review on energy-saving optimization methods for robotic and automatic systems". *Robotics,* **6**(4), p. 39.

[5] Yin, H., Liu, J., and Yang, F., 2019. "Hybrid structure design of lightweight robotic arms based on carbon fiber reinforced plastic and aluminum alloy". *IEEE Access,* **7**, pp. 64932–64945.

[6] Khalaf, P., and Richter, H., 2016. "Parametric optimization of stored energy in robots with regenerative drive systems". In IEEE Int. Conf. on Advanced Intel. Mechatronics, IEEE, pp. 1424–1429.

[7] Scalera, L., Palomba, I., Wehrle, E., Gasparetto, A., and Vidoni, R., 2019. "Natural motion for energy saving in robotic and mechatronic systems". *Applied Sciences,* **9**(17), p. 3516.

[8] Scalera, L., Carabin, G., Vidoni, R., and Wongratanaphisan, T., 2019. "Energy efficiency in a 4-DOF parallel robot featuring compliant elements". *International Journal of Mechanics and Control,* **20**(2).

[9] Iwamura, M., and Schiehlen, W., 2016. "Control and experiments with energy-saving scara robots". In Symposium on Robot Design, Dynamics and Control, Springer, pp. 153–161.

[10] Deepak, S. R., and Ananthasuresh, G., 2012. "Perfect static balance of linkages by addition of springs but not auxiliary bodies". *J. of Mech. and Rob.,* **4**(2), p. 021014.

[11] Richiedei, D., and Trevisani, A., 2020. "Optimization of the energy consumption through spring balancing of servo-actuated mechanisms". *Journal of Mechanical Design,* **142**(1).

This is a pre-print of the article: F. Vidussi, P. Boscariol, L. Scalera, A. Gasparetto
Local and trajectory-based indexes for task-related energetic performance optimization of robotic manipulators
Journal of Mechanisms and Robotics, 2021, 13.2: 021018 `https://doi.org/10.1115/1.4049972`

[12] Karimi Eskandary, P., Belzile, B., and Angeles, J., 2019. "Trajectory-planning and normalized-variable control for parallel pick-and-place robots". *Journal of Mechanisms and Robotics,* **11**(3).

[13] Boscariol, P., and Richiedei, D., 2019. "Energy-efficient design of multipoint trajectories for cartesian robots". *The Int. Journal of Advanced Manufacturing Technology,* **102**(5-8), pp. 1853–1870.

[14] Carabin, G., Vidoni, R., and Wehrle, E., 2018. "Energy saving in mechatronic systems through optimal point-to-point trajectory generation via standard primitives". In Int. Conf. of IFToMM ITALY, Springer, pp. 20–28.

[15] Paes, K., Dewulf, W., Vander Elst, K., Kellens, K., and Slaets, P., 2014. "Energy efficient trajectories for an industrial ABB robot". *Proc. Cirp,* **15**, pp. 105–110.

[16] Ho, P. M., Uchiyama, N., Sano, S., Honda, Y., Kato, A., and Yonezawa, T., 2014. "Simple motion trajectory generation for energy saving of industrial machines". *SICE J. of Contr., Meas., Syst. Int.,* **7**(1), pp. 29–34.

[17] Patel, S., and Sobh, T., 2015. "Manipulator performance measures-a comprehensive literature survey". *Journ. of Int. & Rob. Systems,* **77**(3-4), pp. 547–570.

[18] Asada, H., 1984. "Dynamic analysis and design of robot manipulators using inertia ellipsoids". In Proc. Int. Conf. on Rob. and Autom., IEEE, pp. 94–102.

[19] Yoshikawa, T., 1985. "Manipulability of robotic mechanisms". *The Int. Jour. of Rob. Research,* **4**(2), pp. 3–9.

[20] Kim, J.-O., and Khosla, K., 1991. "Dexterity measures for design and control of manipulators". In Int. Workshop on Int. Rob. and Syst., IEEE/RSJ, pp. 758–763.

[21] Klein, C. A., and Blaho, B. E., 1987. "Dexterity measures for the design and control of kinematically redundant manipulators". *Int. J. of Rob. Res.,* **6**(2), pp. 72–83.

[22] Tanev, T., and Stoyanov, B., 2000. "On the performance indexes for robot manipulators". *Problems of engineering cybernetics and robotics,* **49**, pp. 64–71.

[23] Kim, S.-G., and Ryu, J., 2003. "New dimensionally homogeneous jacobian matrix formulation by three end-effector points for optimal design of parallel manipulators". *IEEE Transactions on Robotics and Automation,* **19**(4), pp. 731–736.

[24] Altuzarra, O., Salgado, O., Petuya, V., and Hernández, A., 2006. "Point-based jacobian formulation for computational kinematics of manipulators". *Mechanism and machine theory,* **41**(12), pp. 1407–1423.

[25] Pond, G., and Carretero, J. A., 2006. "Formulating jacobian matrices for the dexterity analysis of parallel manipulators". *Mechanism and Machine Theory,* **41**(12), pp. 1505–1519.

[26] Ruggiu, M., 2010. "Kinematic and dynamic analysis of a two-degree-of-freedom spherical wrist". *Journal of Mechanisms and Robotics,* **2**(3), p. 031006.

[27] Merlet, J.-P., 2006. "Jacobian, manipulability, condition number, and accuracy of parallel robots". *Journal of Mechanical Design,* **128**(1), pp. 199–206.

[28] Li, Q., Zhang, N., and Wang, F., 2017. "New indices for optimal design of redundantly actuated parallel manipulators". *Journal of Mech. and Rob.,* **9**(1), p. 011007.

[29] Boschetti, G., and Trevisani, A., 2018. "Cable robot performance evaluation by wrench exertion capability". *Robotics,* **7**(2), p. 15.

[30] Khalilpour, S. A., Loloei, A. Z., Taghirad, H. D., and Masouleh, M. T., 2013. "Feasible kinematic

This is a pre-print of the article: F. Vidussi, P. Boscariol, L. Scalera, A. Gasparetto
Local and trajectory-based indexes for task-related energetic performance optimization of robotic manipulators
Journal of Mechanisms and Robotics, 2021, 13.2: 021018 https://doi.org/10.1115/1.4049972

sensitivity in cable robots based on interval analysis". In *Cable-Driven Parallel Robots*. Springer, pp. 233–249.

[31] Seriani, S., Gallina, P., and Gasparetto, A., 2014. "A performance index for planar repetitive workspace robots". *Journal of Mech. and Rob.,* **6**(3), p. 031005.

[32] Rosenstein, M. T., and Grupen, R. A., 2002. "Velocity-dependent dynamic manipulability". In Proc. Int. Conf. on Rob. and Autom., Vol. 3, IEEE, pp. 2424–2429.

[33] Kurazume, R., and Hasegawa, T., 2006. "A new index of serial-link manipulator performance combining dynamic manipulability and manipulating force ellipsoids". *IEEE Trans. on Rob.,* **22**(5), pp. 1022–1028.

[34] Dos Santos, R. R., Steffen, V., and Saramago, S. d. F. P., 2010. "Optimal task placement of a serial robot manipulator for manipulability and mechanical power optimization". *Int. Inform. Management,* **2**(09), p. 512.

[35] Boschetti, G., Rosa, R., and Trevisani, A., 2013. "Optimal robot positioning using task-dependent and direction-selective performance indexes: General definitions and application to a parallel robot". *Rob. and Comp.-Int. Manuf.,* **29**(2), pp. 431–443.

[36] Ur-Rehman, R., Caro, S., Chablat, D., and Wenger, P., 2010. "Multi-objective path placement optimization of parallel kinematics machines based on energy consumption, shaking forces and maximum actuator torques: Application to the orthoglide". *Mechanism and Machine Theory,* **45**(8), pp. 1125–1141.

[37] Boscariol, P., Scalera, L., and Gasparetto, A., 2019. "Task-Dependent Energetic Analysis of a 3 dof Industrial Manipulator". In Int. Conf. on Robotics in Alpe-Adria Danube Region, Springer, pp. 162–169.

[38] Park, R. H., 1929. "Two-reaction theory of synchronous machines generalized method of analysis-part i". *Transactions of the American Institute of Electrical Engineers,* **48**(3), pp. 716–727.

[39] Paryanto, Brossog, M., Bornschlegl, M., Franke, J., et al., 2015. "Reducing the energy consumption of industrial robots in manufacturing systems". *The Int. Journ. of Adv. Manuf. Techn.,* **78**(5-8), pp. 1315–1328.

[40] Meike, D., Pellicciari, M., and Berselli, G., 2013. "Energy efficient use of multirobot production lines in the automotive industry: Detailed system modeling and optimization". *IEEE Trans. on Automation Science and Engineering,* **11**(3), pp. 798–809.

[41] Al-Naseem, O., Erickson, R. W., and Carlin, P., 2000. "Prediction of switching loss variations by averaged switch modeling". In 15th Applied Power Electronics Conf. and Exp., Vol. 1, IEEE, pp. 242–248.

[42] Biagiotti, L., and Melchiorri, C., 2008. *Trajectory planning for automatic machines and robots*. Springer Science & Business Media.

[43] Richiedei, D., and Trevisani, A., 2016. "Analytical computation of the energy-efficient optimal planning in rest-to-rest motion of constant inertia systems". *Mechatronics,* **39**, pp. 147–159.

This is a pre-print of the article: F. Vidussi, P. Boscariol, L. Scalera, A. Gasparetto
Local and trajectory-based indexes for task-related energetic performance optimization of robotic manipulators
Journal of Mechanisms and Robotics, 2021, 13.2: 021018 https://doi.org/10.1115/1.4049972